

Errata on the Calculation of Hot Gas Properties in a Few Li Jiang-Tao's Papers

JIANG-TAO LI¹ AND RUI HUANG^{2,1}

¹*Department of Astronomy, University of Michigan, 311 West Hall, 1085 S. University Ave, Ann Arbor, MI, 48109-1107, U.S.A.*

²*Department of Astronomy, Tsinghua University, Beijing 100084, China*

ABSTRACT

This is a combination of the errata of seven papers published between 2008 and 2016 with Jiang-Tao Li (JTL) as the first author. All the problems are caused by two mistakes in the original scripts written by JTL used to calculate the physical parameters of the hot gas from X-ray spectral analysis with a thermal plasma code. The mistakes will result in an overestimate of some parameters, such as the electron number density and hot gas mass by a factor of $\sqrt{10} \approx 3.162$, and an overestimate of the thermal pressure by a factor of ≈ 2.725 . JTL apologizes to the community for the inconvenience caused by these mistakes. We present an update on the text, numbers, figures, and tables of all the seven papers affected by these mistakes. Other papers led by JTL or co-authored papers are not affected.

1. THE MISTAKES

Jiang-Tao Li (JTL) made a mistake in unit conversion when calculating the emission measure and electron number density from the normalization of a fitted thermal plasma model (e.g., MEKAL or APEC). Below we describe where the mistakes come from.

The normalization of a thermal plasma model (e.g., MEKAL or APEC) is often defined as:

$$norm = \frac{10^{-14}}{4\pi[D_A(1+z)]^2} \int n_e n_H dV, \quad (1)$$

where D_A is the angular diameter distance to the source in unit of cm, n_e and n_H are the number densities of electron and Hydrogen in unit of cm^{-3} .

We convert the measured $norm$ to the volume emission measure EM and then to the Hydrogen number density and other physical parameters. The original formulae in the script are:

$$EM = 4\pi norm d^2 / pc, \quad (2)$$

$$n_H = \sqrt{EM/V_{emit}/\mathcal{R}_{n_e n_H}}, \quad (3)$$

where d is the distance to a local galaxy in Mpc (we do not consider the $1+z$ term for local galaxies), $pc = 3.086$ is in unit of 10^{18} cm, V_{emit} is the volume of the X-ray emitting region in unit of kpc^3 , and $\mathcal{R}_{n_e n_H}$ is the electron to Hydrogen number ratio depending on the metallicity and ionization state of the gas. In some early papers, we have assumed $\mathcal{R}_{n_e n_H} = 1$ (Li et al. 2008, 2009; Li & Wang 2013), while in later papers, $\mathcal{R}_{n_e n_H}$ has been calculated based on the measured metallicity (Li 2015a; Li et al. 2016a,b). As $\mathcal{R}_{n_e n_H}$ is very close to 1 (~ 1.2 for fully ionized solar abundance gas) and the actual value of it does not affect the result significantly, we still follow the original assumption of it in the corresponding papers. Here the derived Hydrogen number density is in unit of $f^{-1/2} \text{cm}^{-3}$, where f is the unknown volume filling factor of the hot gas. The exact forms of the above equations depend on the adopted unit of the parameters. In Eq. 2, JTL has missed a factor of 10. The correct formula should actually be:

$$EM = 4\pi norm d^2 / pc / 10. \quad (4)$$

This mistake will cause an overestimate of the emission measure by a factor of 10 and an overestimate of the Hydrogen and electron number densities by a factor of $\sqrt{10}$. All the related parameters, such as the thermal pressure, the mass and thermal energy of hot gas, are also overestimated by a factor of $\sqrt{10}$.

Corresponding author: Jiang-Tao Li

pandataotao@gmail.com

Furthermore, JTL also adopted an inaccurate formula when calculating the thermal pressure of hot gas (in unit of $f^{-1/2}$ eV/cm³):

$$P_{them} = 10^7 n_e k_B T, \quad (5)$$

where k_B is the Boltzmann constant (8.6173325×10^{-5} eV/K), n_e is in unit of $f^{-1/2}$ cm⁻³, and T is the hot gas temperature in unit of keV. The formula itself is not wrong, but contains an inaccurate relation converting the temperature unit from eV to Kelvin (JTL has simply assumed 1 eV = 10⁴ K). A more accurate form of Eq. 5 should be:

$$P_{them} = 10^3 n_e k_B T, \quad (6)$$

where $k_B T$ as a single parameter, instead of T , is in unit of keV. This mistake will result in an underestimate of the thermal pressure by a factor of $10^4/k_B \approx 1.160$.

The combined effect of the above two mistakes is an overestimate of the electron and Hydrogen number densities, the mass and thermal energy of the hot gas by a factor of $\sqrt{10} \approx 3.162$, and an overestimate of the thermal pressure by a factor of $\sqrt{10}/1.160 \approx 2.725$. The case of the radiative cooling timescale t_{cool} is more complicated as it was estimated in different ways in different papers. In some early papers (Li et al. 2008, 2009; Li & Wang 2013), t_{cool} is obtained by directly dividing the thermal energy with the observed X-ray luminosity, so it is $\propto n_e$ and also overestimated by a factor of ≈ 3.162 . In Li et al. (2014), we also present the radiative cooling rate \dot{M}_{cool} in Fig.1b of that paper, which is obtained by dividing the total hot gas mass in the CGM M_{hot} with t_{cool} . As M_{hot} and t_{cool} in this paper are both overestimated by a factor of $\sqrt{10}$, \dot{M}_{cool} in Fig.1b of Li et al. (2014) and the related discussions are not affected by this mistake. We therefore do not issue an erratum of Li et al. (2014). However, in some later papers such as Li et al. (2016b), t_{cool} is obtained from the cooling function, so it is $\propto n_e^{-1}$ and has been underestimated by a factor of ≈ 3.162 . We also calculated the radiative cooling rate \dot{M}_{cool} in these later papers, which is $\propto n_e^2$ so has been overestimated by a factor of 10. Other directly measured hot gas parameters, such as the X-ray luminosity, and sometimes temperature and metallicity, are not affected by these mistakes. We also want to emphasize that in the two latter CGM-MASS papers (Li et al. 2017, 2018), we use a different method to calculate the derived physical parameters of the hot gas from those adopted in CGM-MASS I (Li et al. 2016b). This new method directly convert the observed X-ray counts rate, metallicity, and radial intensity profile to the radial distribution of physical parameters, so is not affected by the above mistakes. There is thus no erratum of Li et al. (2017, 2018).

These mistakes were not noticed by JTL, as the deviations of the estimated hot gas parameters are not quite significant, and the estimate itself is often highly uncertain due to the large errors of the measurement and many assumptions (e.g., the unknown volume filling factor f). A graduate student, Rui Huang (RH), working with JTL has recently found the mistakes in a careful examination of the early scripts written by JTL. As the scripts have been used for many years without an update, seven of JTL's first author papers published from 2008 to 2016 have been more or less affected by these mistakes. JTL would like to apologize to the community for the inconvenience caused by these mistakes. We herein present errata of all these seven papers, with the corrected text marked in red. All these errata will also be separately submitted to the corresponding journals.

2. ERRATUM: ‘‘Chandra observation of the edge-on spiral NGC 5775: probing the hot galactic disc/halo connection’’ (2008, MNRAS, 390, 59)

- The EM in Table 3 of Li et al. (2008) should be updated to those in Table 1 of this erratum.
- Physical parameters in Table 4 of Li et al. (2008) should be updated to those in Table 2 of this erratum.
- In section 4.3, 5th paragraph of Li et al. (2008). The following sentence should be changed to:

‘‘The hot-gas pressure in the halo is $\sim 3.8 \times 10^{-13}$ dyn cm⁻² for each of the two components, derived from the hot-gas parameters listed in Table 4.’’

Table 1. Spectral Fitting Parameters (Table 3 of Li et al. (2008))

| Region | Model | N_H | T_{Low} | EM_{Low} | T_{High} | EM_{High} | Γ | $\chi^2/d.o.f.$ |
|--------|-------------|-------------------------------|------------------------|------------------------------------|--------------------------|------------------------------------|------------------------|-----------------|
| | | (10^{20} cm^{-2}) | (keV) | ($\text{cm}^{-6} \text{ kpc}^3$) | (keV) | ($\text{cm}^{-6} \text{ kpc}^3$) | | |
| (1) | (2) | (3) | (4) | (5) | (6) | (7) | (8) | (9) |
| ULX | PL | 286^{+50}_{-37} | - | - | - | - | $1.82^{+0.31}_{-0.22}$ | 50.6/44 |
| Disk | Mekal+PL | $53.9^{+10.5}_{-3.9}$ | $0.19^{+0.01}_{-0.01}$ | 0.131 | - | - | 1.34 (fixed) | 92.9/74 |
| Halo | Mekal+Mekal | 3.48 (fixed) | 0.17 (< 0.19) | 0.0047 | $0.57^{+0.015}_{-0.015}$ | 0.0017 | - | 70.4/69 |

NOTE—(1) Regions from which spectra were extracted; (2) Mekal = XSPEC MEKAL thermal plasma model, PL = Power Law; (3) Hydrogen absorption column density; (4)(6) Temperatures of the thermal components; (5)(7) Emission measure of the thermal components; (8) Photon index of the PL component; (9) Statistics of the spectral fit. Note that the last column is calculated with the sky background, while the spectra shown in Fig. 8 is after sky background subtraction.

Table 2. Hot Halo Gas Parameters (Table 4 of Li et al. (2008))

| Parameters | Low T Component | High T Component |
|--|-----------------|------------------|
| Volume Filling Factor | 0.2 | 0.8 |
| Number Density (10^{-3} cm^{-3}) | 1.4 | 0.41 |
| Mass ($10^8 M_\odot$) | 0.76 | 0.92 |
| Thermal Energy (10^{56} ergs) | 0.44 | 1.7 |
| Cooling Time Scale (10^9 yr) | 0.63 | 4.1 |

NOTE—These quantities are derived from the parameters listed in Table 3, assuming that the filling factor of the hot gas is f_{high} (f_{low}) for the high (low) temperature component with $f_{high} + f_{low} \sim 1$, and that the hot gas is located in a cylinder with a diameter of D_{25} .

3. ERRATUM: “Dynamic S0 galaxies: a case study of NGC 5866” (2009, ApJ, 706, 693)

- In section 3.2, the last paragraph of Li et al. (2009), the following sentence should be changed to: “The corresponding emission measure of the hot gas is $\sim 0.007 \text{ cm}^{-6} \text{ kpc}^3$.”
- In section 4.2, the first paragraph of Li et al. (2009), the following sentence should be changed to: “we estimate the mean **electron** density, thermal pressure, and radiative cooling timescale of the hot gas as $\sim 0.021 \text{ cm}^{-3}$, $\sim 3.6 \times 10^{-12} \text{ dyne cm}^{-2}$, and $\sim 4.7 \times 10^7 \text{ yr}$. The total hot gas mass is $\sim 10^7 M_\odot$.”
- In section 4.3, the first paragraph of Li et al. (2009), the estimate of the warm gas properties is based on the assumption of pressure balance between hot gas and warm gas, so also indirectly affected by the mistakes. However, as the pressure balance assumption itself is highly uncertain, and the estimate of the warm gas properties is just accurate on order of magnitude, we will not change the numbers in this paragraph. The following discussions will not be affected.

4. ERRATUM: “Chandra survey of nearby highly inclined disc galaxies - I. X-ray measurements of galactic coronae” (2013, MNRAS, 428, 2085)

The following tables should be updated accordingly. We also slightly changed the format of the table, i.e., use $value \pm limit$ to replace $value_{-lower}^{+upper}$ when the lower and upper limits of a parameter equal to each other.

- Physical parameters in Table 7 of Li & Wang (2013) should be updated to those in Table 3 of this erratum.
- Physical parameters in Table 8 of Li & Wang (2013) should be updated to those in Table 4 of this erratum.
- Physical parameters in Table 9 of Li & Wang (2013) should be updated to those in Table 5 of this erratum.

• Fig. 10 of Li & Wang (2013) should be updated to Fig. 1 of this erratum. An updated calculation indicates the correlation coefficient of the $i - n_e$ relation is $|r_s| < 0.3$, so we remove it from the plot. Furthermore, in §5.2.2, the following sentence

“As an example (the most significant dependence on i), Fig. 10(a) shows that n_e seems to be slightly correlated with i ; but the correlation is only marginal (-0.31 ± 0.12) and probably dominated by only a few galaxies with high n_e values.”

should be changed to:

“An example is shown in Fig. 10(a), where n_e does not show a significant correlation with i .”

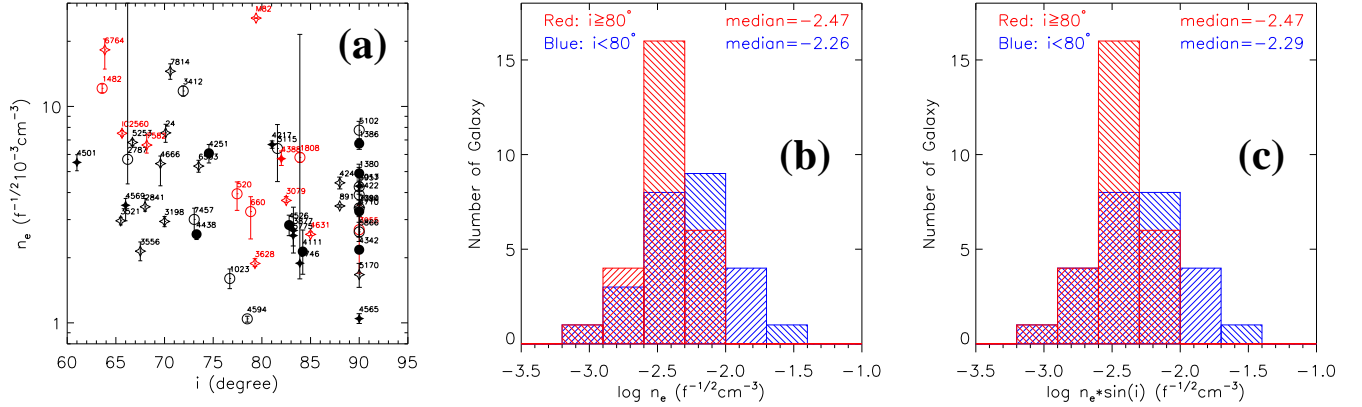


Figure 1. (Fig.10 of Li & Wang (2013)) (a) Hot gas density (n_e) vs. inclination angle (i), where the symbols have the same meanings as those in Fig. 8. (b) n_e distributions of highly ($i \geq 80^\circ$) and moderately ($i < 80^\circ$) inclined galaxies, where the median value of $\log n_e$ for each subsamples is given at the upper right corner. (c) Similar to (b), but with a simple geometry correction for the volume used in the calculation of n_e .

5. ERRATUM: “Do we detect the galactic feedback material in X-ray observations of nearby galaxies? - A case study of NGC 5866” (2015, MNRAS, 453, 1062)

• EM in Table 1 of Li (2015a) should be updated to those in Table 6 of this erratum.

• Section 3.1, 2nd paragraph. The following sentences should be changed to:

“The densities of the inner and outer halos are $\sim 3.8 \times 10^{-3} f^{-1/2} \text{ cm}^{-3}$ and $\sim 1.1 \times 10^{-3} f^{-1/2} \text{ cm}^{-3}$, respectively, where f is the poorly known volume filling factor. The total mass of hot gas contained in the inner and outer halos are both $\sim 3 \times 10^7 f^{1/2} M_\odot$. As the metallicity in the outer halo cannot be well constrained, we only estimate the total Fe mass contained in the inner halo, which is $\sim 6 \times 10^4 f^{1/2} M_\odot$.”

• Section 3.1, 3rd paragraph. The following sentences should be changed to:

“Within this timescale, there are $\sim 2 \times 10^4 M_\odot$ Fe injected into the ISM by Type Ia SNe (assuming each Type Ia SN eject $\sim 0.7 M_\odot$ Fe; Nomoto, Thielemann & Yokoi 1984), about **three times** smaller than what we have detected in the inner halo, assuming the volume filling factor $f \sim 1$.”

“Within this timescale, the total Fe injected by Type Ia SNe is $\sim 10^7 M_\odot$, **more than two orders of magnitude** higher than what we have detected.”

6. ERRATUM: “XMM-Newton large program on SN1006 - I: Methods and initial results of spatially-resolved spectroscopy” (2015, MNRAS, 453, 3953)

• Fig. 5 of Li et al. (2015b) should be updated to Fig. 2 of this erratum. Only the scale of the vertical axis has been changed.

• n_e in Table 4 of Li et al. (2015b) should be updated to those in Table 7 of this erratum.

• Fig. 9(c) and (d) of Li et al. (2015b) should be updated to the left and right panels of Fig. 3 of this erratum, respectively. While the n_e map (right panel) only has the scale of the color bar changed, the t_{ion} map (left panel)

Table 3. Hot Gas Properties from the 1-T Model Fits (Table 7 of Li & Wang (2013))

| Name | L_{hot} (10^{38} ergs/s) (1) | T_{hot} (keV) (2) | EM ($10^{-2} \text{ cm}^{-6} \text{ kpc}^3$) (3) | n_e ($f^{-1/2} 10^{-3} \text{ cm}^{-3}$) (4) | M_{hot} ($f^{1/2} 10^8 M_{\odot}$) (5) | E_{hot} ($f^{1/2} 10^{55}$ ergs) (6) | t_{cool} ($f^{1/2} 2 \text{ Gyr}$) (7) |
|---------|---|--|--|--|--|---|--|
| IC2560 | 66.34 ± 4.01 | 0.3 | 2.35 ± 0.14 | 2.52 ± 0.08 | 2.31 ± 0.07 | 13.2 ± 4.4 | 0.63 ± 0.21 |
| M82 | 68.76 ^{+0.29} _{-0.30} | 0.611 ± 0.003 | 1.79 ± 0.01 | 9.48 ± 0.02 | 0.4669 ± 0.0010 | 5.43 ± 0.03 | 0.251 ± 0.002 |
| NGC0024 | 1.70 ± 0.33 | 0.3 | 0.049 ± 0.009 | 4.25 ± 0.41 | 0.028 ± 0.003 | 0.16 ± 0.06 | 0.30 ± 0.12 |
| NGC0520 | 19.06 ^{+3.71} _{-6.22} | 0.29 ^{+0.05} _{-0.03} | 0.36 ^{+0.10} _{-0.11} | 1.76 ^{+0.24} _{-0.28} | 0.50 ^{+0.07} _{-0.08} | 2.8 ^{+0.6} _{-0.5} | 0.46 ^{+0.13} _{-0.17} |
| NGC0660 | 11.73 ^{+3.05} _{-2.03} | 0.52 ^{+0.11} _{-0.13} | 0.15 ^{+0.05} _{-0.08} | 1.46 ^{+0.25} _{-0.37} | 0.25 ^{+0.04} _{-0.06} | 2.5 ^{+0.7} _{-0.9} | 0.68 ^{+0.26} _{-0.27} |
| NGC0891 | 22.26 ^{+0.50} _{-0.51} | 0.34 ± 0.01 | 0.57 ± 0.01 | 1.26 ± 0.02 | 1.11 ± 0.01 | 7.1 ± 0.1 | 1.01 ± 0.03 |
| NGC1023 | 2.81 ^{+0.59} _{-0.70} | 0.26 ^{+0.03} _{-0.02} | 0.055 ^{+0.012} _{-0.011} | 0.71 ^{+0.08} _{-0.07} | 0.19 ± 0.02 | 0.94 ^{+0.14} _{-0.12} | 1.07 ^{+0.27} _{-0.30} |
| NGC1380 | 38.95 ^{+3.35} _{-3.64} | 0.33 ± 0.02 | 0.65 ^{+0.09} _{-0.06} | 2.19 ^{+0.14} _{-0.11} | 0.73 ^{+0.05} _{-0.04} | 4.5 ^{+1.2} _{-0.3} | 0.37 ^{+0.05} _{-0.04} |
| NGC1386 | 14.86 ^{+1.17} _{-1.97} | 0.26 ± 0.01 | 0.29 ± 0.03 | 3.00 ^{+0.16} _{-0.18} | 0.24 ± 0.01 | 1.18 ± 0.09 | 0.25 ^{+0.03} _{-0.04} |
| NGC1482 | 37.21 ^{+3.05} _{-3.31} | 0.38 ± 0.03 | 0.57 ± 0.05 | 4.09 ^{+0.19} _{-0.18} | 0.35 ± 0.02 | 2.5 ± 0.2 | 0.21 ± 0.03 |
| NGC1808 | 9.09 ^{+0.92} _{-1.02} | 0.58 ^{+0.03} _{-0.06} | 0.12 ± 0.01 | 1.77 ± 0.09 | 0.168 ± 0.009 | 1.8 ^{+0.1} _{-0.2} | 0.64 ^{+0.08} _{-0.10} |
| NGC2787 | 1.77 ^{+1.85} _{-1.32} | 0.18 ^{+0.11} _{-0.18} | 0.12 ^{+3.21} _{-0.06} | 2.54 ^{+33.46} _{-0.58} | 0.12 ^{+1.56} _{-0.03} | 0.41 ^{+5.47} _{-0.43} | 0.74 ^{+9.84} _{-0.94} |
| NGC2841 | 19.37 ^{+2.77} _{-3.17} | 0.41 ^{+0.07} _{-0.04} | 0.47 ^{+0.09} _{-0.04} | 1.53 ^{+0.14} _{-0.07} | 0.76 ^{+0.07} _{-0.03} | 6.0 ^{+1.2} _{-0.6} | 0.98 ^{+0.24} _{-0.19} |
| NGC3079 | 65.90 ^{+3.61} _{-3.77} | 0.51 ± 0.02 | 1.64 ^{+0.14} _{-0.07} | 1.55 ^{+0.06} _{-0.03} | 2.66 ^{+0.11} _{-0.05} | 25.8 ^{+1.6} _{-1.2} | 1.25 ^{+0.10} _{-0.09} |
| NGC3115 | 0.41 ^{+0.13} _{-0.19} | 0.08 ^{+0.04} _{-0.08} | 0.23 ^{+0.13} _{-0.14} | 2.85 ^{+0.83} _{-0.85} | 0.20 ± 0.06 | 0.31 ^{+0.17} _{-0.32} | 2.36 ^{+1.49} _{-2.69} |
| NGC3198 | 15.62 ± 1.69 | 0.3 | 0.42 ± 0.05 | 1.31 ± 0.07 | 0.79 ± 0.04 | 4.5 ± 1.5 | 0.91 ± 0.32 |
| NGC3384 | 7.18 ± 1.26 | 0.3 | 0.15 ± 0.03 | 1.31 ± 0.12 | 0.28 ± 0.02 | 1.6 ± 0.5 | 0.69 ± 0.27 |
| NGC3412 | 9.82 ± 1.07 | 0.3 | 0.26 ± 0.03 | 5.25 ± 0.28 | 0.124 ± 0.007 | 0.71 ± 0.24 | 0.23 ± 0.08 |
| NGC3521 | 20.24 ^{+1.35} _{-1.37} | 0.36 ^{+0.03} _{-0.02} | 0.52 ± 0.04 | 1.33 ^{+0.05} _{-0.06} | 0.97 ± 0.04 | 6.6 ^{+0.6} _{-0.4} | 1.04 ^{+0.12} _{-0.10} |
| NGC3556 | 5.73 ^{+1.01} _{-1.16} | 0.33 ± 0.02 | 0.15 ± 0.03 | 0.80 ± 0.08 | 0.45 ^{+0.05} _{-0.04} | 2.8 ± 0.3 | 1.56 ^{+0.33} _{-0.36} |
| NGC3628 | 24.45 ^{+1.86} _{-2.06} | 0.32 ± 0.01 | 0.61 ^{+0.06} _{-0.04} | 0.75 ^{+0.04} _{-0.02} | 2.01 ^{+0.11} _{-0.07} | 12.4 ^{+0.8} _{-0.7} | 1.61 ± 0.16 |
| NGC3877 | 1.21 ^{+0.61} _{-0.68} | 0.30 ^{+0.05} _{-0.06} | 0.030 ^{+0.017} _{-0.013} | 0.78 ^{+0.22} _{-0.17} | 0.097 ^{+0.027} _{-0.021} | 0.56 ^{+0.19} _{-0.16} | 1.47 ^{+0.88} _{-0.93} |
| NGC3955 | 10.77 ^{+3.67} _{-6.27} | 0.31 ^{+0.29} _{-0.05} | 0.18 ^{+0.11} _{-0.14} | 1.20 ^{+0.36} _{-0.44} | 0.38 ^{+0.11} _{-0.14} | 2.2 ^{+2.2} _{-0.9} | 0.65 ^{+0.68} _{-0.46} |
| NGC3957 | 19.68 ± 2.95 | 0.3 | 0.42 ± 0.06 | 1.89 ± 0.14 | 0.55 ± 0.04 | 3.1 ± 1.1 | 0.50 ± 0.19 |
| NGC4013 | 14.47 ± 1.39 | 0.3 | 0.39 ± 0.04 | 1.59 ± 0.08 | 0.61 ± 0.03 | 3.5 ± 1.2 | 0.77 ± 0.27 |
| NGC4111 | 3.74 ^{+1.36} _{-2.13} | 0.44 ^{+0.12} _{-0.10} | 0.052 ^{+0.027} _{-0.023} | 0.76 ^{+0.20} _{-0.16} | 0.17 ± 0.04 | 1.4 ^{+0.6} _{-0.5} | 1.23 ^{+0.65} _{-0.80} |
| NGC4217 | 20.35 ± 1.59 | 0.3 | 0.55 ± 0.04 | 2.08 ± 0.08 | 0.65 ± 0.03 | 3.7 ± 1.3 | 0.58 ± 0.20 |
| NGC4244 | 1.08 ± 0.14 | 0.3 | 0.030 ± 0.004 | 1.98 ± 0.12 | 0.037 ± 0.002 | 0.21 ± 0.07 | 0.63 ± 0.23 |
| NGC4251 | 23.05 ± 4.52 | 0.3 | 0.45 ± 0.09 | 2.71 ± 0.27 | 0.41 ± 0.04 | 2.3 ± 0.8 | 0.32 ± 0.13 |
| NGC4342 | 85.89 ^{+2.89} _{-2.92} | 0.53 ± 0.02 | 1.15 ± 0.04 | 1.23 ± 0.02 | 2.32 ± 0.04 | 23.4 ± 0.8 | 0.87 ± 0.04 |
| NGC4388 | 44.31 ^{+7.00} _{-5.55} | 0.61 ^{+0.04} _{-0.05} | 1.17 ^{+0.20} _{-0.16} | 2.11 ^{+0.18} _{-0.15} | 1.37 ^{+0.12} _{-0.10} | 15.8 ± 1.8 | 1.13 ^{+0.22} _{-0.19} |
| NGC4438 | 52.76 ^{+3.65} _{-3.95} | 0.52 ± 0.03 | 0.72 ^{+0.05} _{-0.08} | 1.06 ^{+0.04} _{-0.06} | 1.69 ^{+0.06} _{-0.09} | 16.9 ^{+1.3} _{-1.4} | 1.01 ^{+0.10} _{-0.11} |
| NGC4501 | 32.12 ^{+5.89} _{-6.13} | 0.56 ^{+0.05} _{-0.07} | 0.82 ± 0.14 | 1.69 ± 0.14 | 1.20 ± 0.10 | 12.8 ^{+1.7} _{-1.9} | 1.26 ^{+0.28} _{-0.31} |
| NGC4526 | 8.84 ^{+1.83} _{-2.05} | 0.27 ^{+0.04} _{-0.02} | 0.17 ± 0.04 | 0.96 ^{+0.11} _{-0.10} | 0.44 ± 0.05 | 2.2 ^{+0.4} _{-0.3} | 0.80 ^{+0.22} _{-0.21} |
| NGC4565 | 8.87 ^{+0.87} _{-0.84} | 0.36 ^{+0.04} _{-0.02} | 0.23 ± 0.02 | 0.47 ^{+0.03} _{-0.02} | 1.21 ^{+0.07} _{-0.06} | 8.3 ^{+0.9} _{-0.7} | 2.97 ^{+0.44} _{-0.37} |
| NGC4569 | 11.43 ^{+1.97} _{-4.45} | 0.56 ± 0.04 | 0.30 ^{+0.04} _{-0.09} | 1.33 ^{+0.04} _{-0.20} | 0.56 ^{+0.04} _{-0.08} | 6.0 ^{+0.6} _{-1.0} | 1.65 ^{+0.34} _{-0.70} |
| NGC4594 | 20.66 ^{+1.08} _{-1.29} | 0.60 ± 0.01 | 0.28 ± 0.02 | 0.41 ± 0.01 | 1.67 ^{+0.05} _{-0.06} | 19.1 ^{+0.7} _{-0.8} | 2.94 ^{+0.19} _{-0.22} |
| NGC4631 | 18.55 ^{+0.66} _{-0.69} | 0.35 ± 0.01 | 0.47 ^{+0.03} _{-0.01} | 0.95 ^{+0.03} _{-0.01} | 1.21 ^{+0.03} _{-0.02} | 8.0 ^{+0.3} _{-0.2} | 1.36 ^{+0.07} _{-0.06} |
| NGC4666 | 27.01 ^{+4.41} _{-11.97} | 0.27 ^{+0.04} _{-0.05} | 0.69 ^{+0.12} _{-0.29} | 1.77 ^{+0.15} _{-0.37} | 0.97 ^{+0.08} _{-0.20} | 5.0 ^{+0.8} _{-1.4} | 0.58 ^{+0.14} _{-0.31} |
| NGC4710 | 6.00 ^{+0.80} _{-3.51} | 0.63 ^{+0.10} _{-0.06} | 0.080 ^{+0.013} _{-0.038} | 1.46 ^{+0.11} _{-0.34} | 0.14 ^{+0.01} _{-0.03} | 1.6 ^{+0.3} _{-0.4} | 0.85 ^{+0.19} _{-0.54} |
| NGC5102 | 0.58 ± 0.11 | 0.3 | 0.013 ± 0.002 | 3.46 ± 0.34 | 0.0091 ± 0.0009 | 0.052 ± 0.018 | 0.28 ± 0.11 |
| NGC5170 | 24.85 ± 6.30 | 0.3 | 0.90 ± 0.23 | 0.74 ± 0.09 | 2.99 ± 0.38 | 17.1 ± 6.1 | 2.18 ± 0.95 |
| NGC5253 | 1.09 ± 0.07 | 0.35 ^{+0.02} _{-0.01} | 0.028 ± 0.002 | 2.55 ^{+0.08} _{-0.09} | 0.0270 ^{+0.0008} _{-0.0009} | 0.179 ^{+0.012} _{-0.008} | 0.52 ^{+0.05} _{-0.04} |
| NGC5422 | 18.36 ± 3.36 | 0.3 | 0.35 ± 0.06 | 1.74 ± 0.16 | 0.49 ± 0.05 | 2.8 ± 1.0 | 0.48 ± 0.19 |
| NGC5746 | 12.87 ^{+4.79} _{-7.50} | 0.16 ^{+0.12} _{-0.16} | 0.46 ^{+9.57} _{-0.14} | 0.84 ^{+8.75} _{-0.13} | 1.35 ^{+14.07} _{-0.21} | 4.2 ^{+43.7} _{-4.2} | 1.03 ^{+10.77} _{-1.20} |
| NGC5775 | 36.35 ^{+3.64} _{-4.25} | 0.38 ^{+0.05} _{-0.04} | 0.92 ^{+0.11} _{-0.19} | 0.79 ^{+0.05} _{-0.08} | 2.87 ^{+0.17} _{-0.30} | 20.9 ^{+2.8} _{-3.0} | 1.82 ^{+0.30} _{-0.34} |
| NGC5866 | 8.96 ^{+1.34} _{-1.56} | 0.31 ^{+0.04} _{-0.03} | 0.15 ± 0.03 | 1.00 ^{+0.11} _{-0.10} | 0.38 ± 0.04 | 2.3 ^{+0.4} _{-0.3} | 0.81 ± 0.18 |
| NGC6503 | 1.54 ^{+0.18} _{-0.21} | 0.42 ^{+0.09} _{-0.06} | 0.039 ± 0.005 | 2.36 ± 0.15 | 0.041 ± 0.003 | 0.32 ^{+0.07} _{-0.05} | 0.67 ^{+0.17} _{-0.14} |
| NGC6764 | 23.48 ^{+6.76} _{-9.84} | 0.75 ^{+0.13} _{-0.11} | 0.70 ^{+0.17} _{-0.26} | 4.47 ^{+0.55} _{-0.83} | 0.38 ^{+0.05} _{-0.07} | 5.5 ^{+1.2} _{-1.3} | 0.74 ^{+0.27} _{-0.36} |
| NGC7090 | 0.44 ^{+0.32} _{-0.38} | 0.44 ^{+0.13} _{-0.14} | 0.009 ^{+0.011} _{-0.005} | 1.53 ^{+0.89} _{-0.41} | 0.015 ^{+0.009} _{-0.004} | 0.13 ^{+0.08} _{-0.05} | 0.91 ^{+0.89} _{-0.87} |
| NGC7457 | 4.97 ± 1.26 | 0.3 | 0.12 ± 0.03 | 1.34 ± 0.17 | 0.21 ± 0.03 | 1.2 ± 0.4 | 0.78 ± 0.34 |
| NGC7582 | 62.94 ^{+10.51} _{-11.88} | 0.67 ^{+0.08} _{-0.07} | 1.64 ^{+0.38} _{-0.27} | 2.60 ^{+0.30} _{-0.21} | 1.55 ^{+0.18} _{-0.13} | 19.7 ^{+3.2} _{-2.7} | 1.00 ± 0.23 |
| NGC7814 | 5.89 ± 0.97 | 0.3 | 0.18 ± 0.03 | 3.88 ± 0.32 | 0.116 ± 0.009 | 0.66 ± 0.23 | 0.36 ± 0.14 |

NOTE—Hot gas properties: (1) absorption corrected 0.5-2 keV luminosity; (2) temperature; (3) volume emission measure; (4) electron number density; (5) mass; (6) thermal energy; (7) radiative cooling timescale. All the parameters are estimated from the 1-T fit with fixed abundance ratio. The temperature is fixed at 0.3 keV for some galaxies with low counting statistic (those without errors). See §3.3 for details.

is further slightly changed compared to the original version, assuming a shell thickness of 0.2 shell radius, consistent with other maps in Fig. 9 (see section 3.2.2 of the text for details).

Table 4. Hot Gas Properties from 1-T Model Fit with Free Abundance Ratio (Table 8 of Li & Wang (2013))

| Name | L_X (10^{38} ergs/s) (1) | T_X (keV) (2) | EM (10^{-2} cm $^{-6}$ kpc 3) (3) | n_e ($f^{-1/2} 10^{-3}$ cm $^{-3}$) (4) | M_{hot} ($f^{1/2} 10^8 M_\odot$) (5) | E_{hot} ($f^{1/2} 10^{55}$ ergs) (6) | t_{cool} ($f^{1/2} 10^7$ Gyr) (7) | Fe/α (8) |
|---------|-------------------------------------|---------------------------|--|---|--|---|--|------------------------|
| M82 | $67.68^{+0.39}_{-0.38}$ | 0.616 ± 0.003 | $1.63^{+0.02}_{-0.01}$ | $9.04^{+0.07}_{-0.03}$ | $0.445^{+0.003}_{-0.002}$ | $5.22^{+0.05}_{-0.03}$ | $0.245^{+0.003}_{-0.002}$ | 0.36 ± 0.01 |
| NGC0891 | $21.85^{+0.48}_{-0.60}$ | 0.32 ± 0.01 | $0.51^{+0.01}_{-0.02}$ | 1.20 ± 0.02 | 1.05 ± 0.02 | 6.4 ± 0.2 | $0.93^{+0.03}_{-0.04}$ | $0.43^{+0.06}_{-0.04}$ |
| NGC1482 | $48.96^{+3.57}_{-2.73}$ | $0.49^{+0.03}_{-0.04}$ | $1.12^{+0.21}_{-0.19}$ | $5.73^{+0.53}_{-0.48}$ | 0.48 ± 0.04 | 4.6 ± 0.5 | 0.30 ± 0.04 | $0.36^{+0.11}_{-0.06}$ |
| NGC1808 | $16.60^{+0.73}_{-0.79}$ | 0.51 ± 0.03 | 0.40 ± 0.04 | 3.23 ± 0.16 | $0.31^{+0.02}_{-0.01}$ | 2.9 ± 0.2 | 0.56 ± 0.05 | $0.34^{+0.06}_{-0.05}$ |
| NGC2841 | $17.75^{+2.48}_{-2.83}$ | $0.38^{+0.04}_{-0.05}$ | $0.39^{+0.08}_{-0.04}$ | $1.39^{+0.14}_{-0.07}$ | $0.69^{+0.07}_{-0.04}$ | 5.0 ± 0.7 | $0.89^{+0.18}_{-0.19}$ | $0.48^{+0.19}_{-0.12}$ |
| NGC3079 | $65.29^{+4.99}_{-4.96}$ | 0.51 ± 0.03 | 1.65 ± 0.14 | $1.53^{+0.07}_{-0.06}$ | 2.67 ± 0.11 | $25.8^{+1.9}_{-1.8}$ | 1.25 ± 0.13 | $0.31^{+0.06}_{-0.05}$ |
| NGC3556 | $5.73^{+1.03}_{-1.18}$ | $0.33^{+0.06}_{-0.03}$ | $0.14^{+0.03}_{-0.02}$ | $0.80^{+0.09}_{-0.07}$ | $0.45^{+0.05}_{-0.04}$ | $2.8^{+0.6}_{-0.4}$ | $1.55^{+0.42}_{-0.38}$ | 0.30 ± 0.12 |
| NGC3628 | $23.32^{+1.08}_{-2.08}$ | $0.30^{+0.01}_{-0.02}$ | $0.47^{+0.05}_{-0.04}$ | $0.66^{+0.04}_{-0.03}$ | $1.77^{+0.09}_{-0.08}$ | $10.2^{+0.7}_{-0.8}$ | $1.39^{+0.11}_{-0.16}$ | $0.45^{+0.48}_{-0.08}$ |
| NGC4342 | $91.18^{+3.53}_{-3.34}$ | 0.54 ± 0.02 | $1.40^{+0.21}_{-0.20}$ | 1.35 ± 0.10 | $2.56^{+0.20}_{-0.18}$ | $26.3^{+2.2}_{-2.0}$ | 0.92 ± 0.08 | $0.79^{+0.16}_{-0.12}$ |
| NGC4526 | $8.77^{+1.77}_{-1.95}$ | $0.26^{+0.07}_{-0.04}$ | 0.16 ± 0.04 | $0.93^{+0.13}_{-0.11}$ | $0.42^{+0.06}_{-0.05}$ | $2.1^{+0.6}_{-0.4}$ | $0.75^{+0.26}_{-0.22}$ | $1.25^{+1.25}_{-0.78}$ |
| NGC4594 | $21.95^{+1.66}_{-1.77}$ | 0.60 ± 0.01 | 0.33 ± 0.08 | $0.45^{+0.05}_{-0.06}$ | $1.83^{+0.21}_{-0.23}$ | $20.9^{+2.5}_{-2.7}$ | $3.03^{+0.42}_{-0.46}$ | $0.81^{+0.29}_{-0.19}$ |
| NGC4631 | $18.16^{+0.72}_{-0.75}$ | 0.33 ± 0.01 | 0.44 ± 0.02 | 0.93 ± 0.02 | $1.18^{+0.02}_{-0.03}$ | $7.5^{+0.2}_{-0.3}$ | 1.31 ± 0.07 | 0.37 ± 0.04 |
| NGC5253 | 1.04 ± 0.08 | 0.32 ± 0.02 | 0.024 ± 0.002 | 2.34 ± 0.10 | 0.025 ± 0.001 | 0.15 ± 0.01 | 0.46 ± 0.05 | $0.48^{+0.08}_{-0.07}$ |
| NGC5866 | $10.59^{+1.43}_{-2.12}$ | $0.137^{+0.004}_{-0.001}$ | $0.17^{+0.05}_{-0.09}$ | $1.05^{+0.14}_{-0.27}$ | $0.40^{+0.06}_{-0.10}$ | $1.1^{+0.1}_{-0.3}$ | $0.32^{+0.06}_{-0.10}$ | < 401.10 |

NOTE—Hot gas properties of the 1-T fit with the Fe/ α ratio set free: (1) extinction corrected 0.5-2 keV luminosity; (2) temperature; (3) volume emission measure; (4) electron number density; (5) mass; (6) thermal energy; (7) radiative cooling timescale; (8) Fe/ α ratio. See §3.3 for details.**Table 5.** Hot Gas Properties from the 2-T Plasma Model (Table 9 of Li & Wang (2013))

| Name | $L_{X,low}$ (10^{38} ergs/s) (1) | $T_{X,low}$ (keV) (2) | $EM_{X,low}$ (10^{-2} cm $^{-6}$ kpc 3) (3) | $L_{X,high}$ (10^{38} ergs/s) (4) | $T_{X,high}$ (keV) (5) | $EM_{X,high}$ (10^{-2} cm $^{-6}$ kpc 3) (6) | $L_{X,total}$ (10^{38} ergs/s) (7) | $T_{X,LW}$ (keV) (8) |
|---------|---|-----------------------------|--|--|------------------------------|---|---|----------------------------|
| NGC0520 | $23.08^{+7.05}_{-20.57}$ | $0.35^{+0.07}_{-0.09}$ | $0.59^{+0.22}_{-0.28}$ | $12.94(< 22.76)$ | $0.77^{+0.27}_{-0.19}$ | $0.36^{+0.49}_{-0.26}$ | $36.1^{+4.5}_{-6.9}$ | $0.50^{+0.14}_{-0.13}$ |
| NGC2841 | $4.20^{+1.40}_{-1.57}$ | $0.11^{+0.03}_{-0.02}$ | $0.62^{+0.79}_{-0.24}$ | $23.56^{+2.31}_{-1.76}$ | $0.49^{+0.04}_{-0.05}$ | $0.60^{+0.06}_{-0.04}$ | $27.7^{+3.0}_{-1.9}$ | $0.43^{+0.04}_{-0.05}$ |
| NGC3079 | $10.28^{+1.49}_{-1.53}$ | $0.12^{+0.02}_{-0.01}$ | 0.90 ± 0.26 | $77.08^{+2.64}_{-3.52}$ | 0.56 ± 0.02 | $1.96^{+0.08}_{-0.09}$ | $87.1^{+2.9}_{-3.6}$ | 0.51 ± 0.02 |
| NGC3521 | $14.00(< 19.75)$ | $0.31^{+0.00}_{-0.05}$ | $0.35^{+0.38}_{-0.15}$ | $7.18(< 14.12)$ | $0.56(< 4.09)$ | $0.19(< 0.33)$ | $21.2^{+1.7}_{-2.0}$ | $0.40^{+1.20}_{-0.22}$ |
| NGC3556 | $3.29^{+0.57}_{-0.66}$ | 0.20 ± 0.03 | 0.096 ± 0.014 | $5.94^{+0.58}_{-0.76}$ | $0.61^{+0.05}_{-0.03}$ | $0.15^{+0.02}_{-0.01}$ | 9.2 ± 0.5 | $0.47^{+0.05}_{-0.03}$ |
| NGC3628 | $7.37^{+5.42}_{-1.71}$ | $0.14^{+0.03}_{-0.02}$ | $0.48^{+0.17}_{-0.13}$ | $25.01^{+2.23}_{-6.76}$ | $0.40^{+0.19}_{-0.03}$ | $0.64^{+0.06}_{-0.07}$ | $34.0^{+2.5}_{-3.8}$ | $0.34^{+0.15}_{-0.03}$ |
| NGC3877 | $0.80(< 1.13)$ | $0.18(< 0.24)$ | $0.027^{+0.231}_{-0.015}$ | $1.38^{+0.28}_{-0.62}$ | $0.59^{+0.13}_{-0.24}$ | $0.035^{+0.009}_{-0.014}$ | $2.1^{+0.3}_{-0.8}$ | $0.44^{+0.11}_{-0.21}$ |
| NGC4388 | $5.61^{+1.81}_{-2.53}$ | $0.09(< 0.12)$ | $1.53^{+1.76}_{-0.87}$ | $51.82^{+3.09}_{-3.31}$ | 0.61 ± 0.04 | $1.34^{+0.10}_{-0.14}$ | $57.4^{+3.1}_{-7.1}$ | $0.56^{+0.04}_{-0.05}$ |
| NGC4501 | $3.06(< 10.59)$ | $0.29(< 0.29)$ | $0.100(< 0.368)$ | $30.48(< 37.90)$ | $0.58^{+0.00}_{-0.08}$ | $0.75^{+0.26}_{-0.19}$ | $33.6^{+8.1}_{-6.9}$ | $0.55^{+0.00}_{-0.10}$ |
| NGC4565 | $4.98(< 8.70)$ | $0.29^{+0.00}_{-0.10}$ | $0.13^{+0.11}_{-0.12}$ | $4.74(< 6.62)$ | $0.56(< 0.56)$ | $0.12(< 0.16)$ | $9.7^{+1.0}_{-1.3}$ | $0.42^{+0.00}_{-0.32}$ |
| NGC4569 | $4.19^{+0.88}_{-1.51}$ | $0.10(< 0.15)$ | $2.48^{+0.63}_{-1.94}$ | $13.22^{+1.13}_{-1.92}$ | $0.56^{+0.02}_{-0.05}$ | 0.34 ± 0.03 | $17.4^{+1.0}_{-2.8}$ | $0.45^{+0.03}_{-0.06}$ |
| NGC4631 | $9.33^{+0.97}_{-1.15}$ | $0.24^{+0.01}_{-0.02}$ | $0.24^{+0.02}_{-0.03}$ | $13.77^{+1.53}_{-1.41}$ | 0.58 ± 0.02 | 0.36 ± 0.04 | $23.3^{+0.9}_{-1.1}$ | 0.44 ± 0.02 |
| NGC5253 | $0.20^{+0.08}_{-0.06}$ | $0.14^{+0.08}_{-0.02}$ | $0.012^{+0.006}_{-0.003}$ | $1.04^{+0.07}_{-0.09}$ | $0.40^{+0.03}_{-0.02}$ | $0.026^{+0.001}_{-0.002}$ | 1.24 ± 0.04 | $0.36^{+0.04}_{-0.02}$ |
| NGC5775 | $6.85^{+9.90}_{-3.81}$ | $0.08(< 0.20)$ | $1.19^{+15.78}_{-0.99}$ | $38.22(< 40.85)$ | $0.37(< 0.61)$ | $0.96^{+0.08}_{-0.71}$ | $45.1^{+3.1}_{-3.6}$ | $0.33(< 0.55)$ |
| NGC6764 | $4.59(< 10.84)$ | $0.30(< 0.30)$ | $0.13(< 0.85)$ | $24.36^{+5.84}_{-19.57}$ | $0.75^{+0.00}_{-0.10}$ | $0.69(< 0.87)$ | $29.6^{+9.8}_{-11.1}$ | $0.68^{+0.00}_{-0.13}$ |
| NGC7582 | $14.61(< 17.97)$ | $0.09(< 0.11)$ | $4.14^{+1.95}_{-3.51}$ | $90.19^{+12.12}_{-28.83}$ | 0.64 ± 0.05 | $2.43^{+0.33}_{-0.32}$ | $105.0^{+11.6}_{-6.8}$ | $0.56^{+0.04}_{-0.05}$ |

NOTE—See §3.3 for details.

- The following sentence in the 2nd from the last paragraph of section 3.2.2 should be changed to:
“As will be discussed in Section 4.2.1, the maximum value of t_{ion} in the SNR interior is typically ~ 1500 yr, consistent with the age of SN1006 ($\sim 10^3$ yr based on historical records; Stephenson 2010).”
- The following sentences in the last paragraph of section 4.2.1 should be changed to:
“Except for the bright rim surrounding the SNR, which is artificial due to the low flux density of the surrounding regions, the whole SNR shell appears to have a low and smooth ionization age of $t_{ion} \lesssim 500$ year. In contrast, all the regions in the SNR interior have $t_{ion} > 500$ year, with the highest $t_{ion} \sim 1500$ year, consistent with the age of SN1006 of $\sim 10^3$ year.”
- The following sentences in section 4.2.2 should be changed to:

Table 6. (Table 1 of Li (2015a)) Hot gas properties from spectral analysis. Spectral analysis results of the ‘inner halo’ region is obtained by jointly fitting the *Suzaku* and *Chandra* spectra (in total 10 free parameters). Spectral analysis results of the ‘outer halo’ region is obtained by fitting the *Suzaku* XIS1 spectrum with a model in which the absorption column density and photon index of the power law, as well as the O and Fe abundances of the hot gas, are all fixed at the values of the inner halo (in total five free parameters). See text for the detail description of the spectral models and Figs 2(a) and (c) for the fitted spectra. All the errors quoted in this table are statistical only, at 90 per cent confidence level. EM is the emission measure of the VAPEC component.

| Parameter | Inner halo | Outer halo |
|-------------------------------------|------------------------------|------------------------|
| $\chi^2/d.o.f.$ | 121.00/135 | 6.59/15 |
| kT (keV) | $0.248^{+0.026}_{-0.027}$ | $0.66^{+0.16}_{-0.11}$ |
| O abundance (solar) | $0.21^{+0.13}_{-0.10}$ | - |
| Fe abundance (solar) | $1.57^{+1.32}_{-0.58}$ | - |
| EM ($\text{cm}^{-6}\text{kpc}^3$) | $0.0053^{+0.0015}_{-0.0012}$ | 0.0015 ± 0.0004 |

“Assuming no CR acceleration in this part so a compression ratio of 4, the ambient ISM density surrounding the ‘NW shell’ should be $n_0 \sim 0.05 \text{ cm}^{-3}$, significantly lower than the values from previous multi-wavelength estimates ($n_0 \sim 0.4 \text{ cm}^{-3}$), which probably indicates the thickness of the SNR shell (0.2 times of the SNR radius) has been overestimated.”

“The northern part of the ‘SNR Interior’ has a clearly lower density of $n_e \lesssim 0.1 \text{ cm}^{-3}$, but ‘SNR Interior 03 and 04’ may form a shell-like structure behind the SW non-thermal rim, apparently extending the ‘NW Shell’.”

“The estimated mass of the shocked X-ray emitting plasma is $\sim 5f^{\frac{1}{2}} M_{\odot}$, where f is the volume filling factor. As discussed in Section 3.2.2, the swept up ambient ISM mass is $\sim 5 M_{\odot}$. Adding the mass of the shocked ejecta, which is quite uncertain but contribute only a small fraction to the mass budget, we could roughly constrain the volume filling factor to be $f \sim 1$ under the adopted geometric model (Section 3.2.2).”

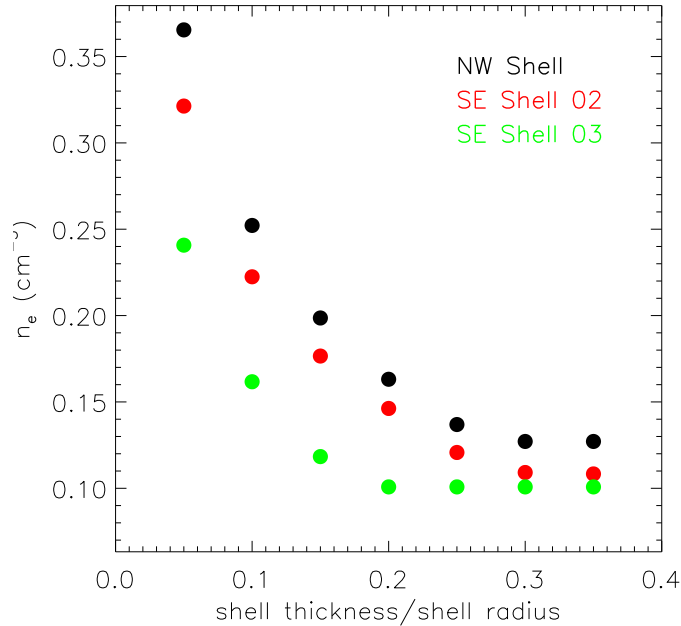


Figure 2. (Fig. 5 of Li et al. (2015b)) Derived post-shock electron number density in several outer regions vs. the assumed thickness of the thermal X-ray emitting shell (in unit of the outer radius of the shell). Region names are denoted in Fig. 7.

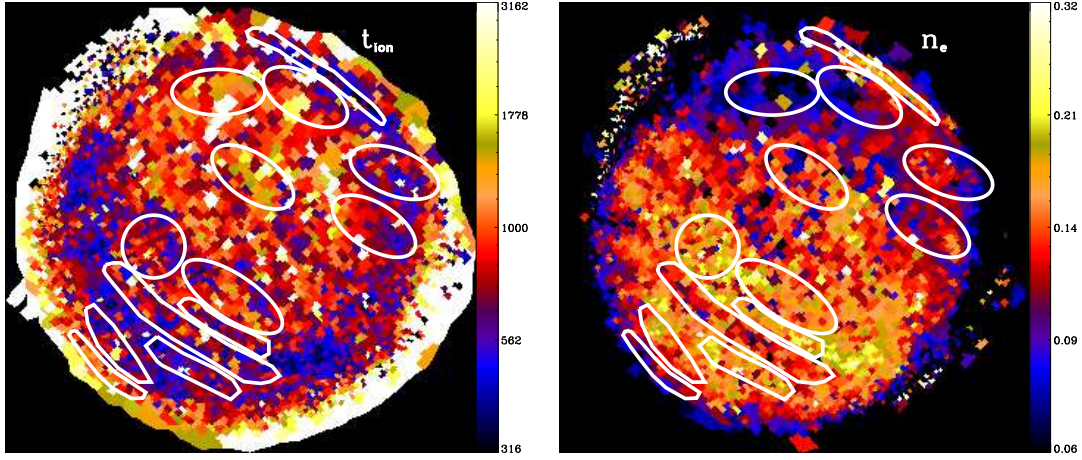


Figure 3. Updated version of Fig. 9(c) and (d) of Li et al. (2015b).

Table 7. Average value of parameters for individual regions (Table 4 of Li et al. (2015b))

| Region | Method | kT | n_e | $\log n_e t$ | O VII $K\delta - \zeta$ | O VII | O VIII | O | Ne | Mg | Si | Fe |
|-------------------|---------|------|------------------|--------------------------------|-------------------------|------------|------------|-------|-------|-------|-------|-------|
| | | keV | cm^{-3} | $\log(\text{cm}^{-3}\text{s})$ | EW | EW | EW | solar | solar | solar | solar | solar |
| NW Shell | Average | 2.25 | 0.16 | 9.56 | 0.18, 23.3 | 0.52, 12.0 | 0.33, 51.9 | 1.13 | 0.85 | 2.20 | 11.06 | 0.23 |
| | Fit | 1.58 | 0.12 | 9.32 | - | - | - | 0.92 | 0.64 | 1.05 | 4.84 | 0.05 |
| SNR Interior 01 | Average | 2.10 | 0.082 | 9.50 | 0.15, 33.1 | 0.57, 15.3 | 0.33, 61.9 | 1.77 | 0.49 | 3.81 | 32.38 | 0.18 |
| | Fit | 2.22 | 0.076 | 9.37 | - | - | - | 0.90 | 0.27 | 1.14 | 7.85 | 0.39 |
| SNR Interior 02 | Average | 1.63 | 0.104 | 9.51 | 0.21, 38.3 | 0.64, 17.8 | 0.41, 74.9 | 2.07 | 0.98 | 5.11 | 30.71 | 0.52 |
| | Fit | 1.56 | 0.098 | 9.35 | - | - | - | 1.05 | 0.44 | 1.69 | 12.36 | 0.83 |
| SNR Interior 03 | Average | 2.47 | 0.108 | 9.40 | 0.17, 23.8 | 0.60, 13.2 | 0.36, 51.5 | 1.44 | 0.50 | 3.42 | 6.95 | 0.25 |
| | Fit | 4.59 | 0.089 | 9.35 | - | - | - | 1.23 | 0.32 | 1.46 | 5.31 | 0.05 |
| SNR Interior 04 | Average | 2.87 | 0.12 | 9.48 | 0.19, 27.0 | 0.60, 10.6 | 0.44, 52.3 | 1.26 | 0.36 | 1.97 | 9.83 | 0.40 |
| | Fit | 2.30 | 0.11 | 9.40 | - | - | - | 1.01 | 0.28 | 1.53 | 7.36 | 0.36 |
| SNR Interior 05 | Average | 1.30 | 0.13 | 9.65 | 0.21, 34.8 | 0.43, 10.8 | 0.37, 59.3 | 1.53 | 0.62 | 3.16 | 20.23 | 0.18 |
| | Fit | 1.12 | 0.11 | 9.60 | - | - | - | 0.80 | 0.35 | 1.26 | 9.31 | 0.28 |
| Dark Belt | Average | 2.06 | 0.14 | 9.49 | 0.17, 25.1 | 0.46, 8.99 | 0.33, 44.7 | 1.06 | 0.39 | 1.10 | 15.33 | 0.73 |
| | Fit | 2.54 | 0.10 | 9.41 | - | - | - | 0.87 | 0.32 | 0.94 | 9.30 | 0.68 |
| Interior Shell 01 | Average | 2.41 | 0.17 | 9.58 | 0.22, 35.9 | 0.40, 8.43 | 0.37, 50.5 | 1.06 | 0.42 | 0.86 | 9.61 | 0.99 |
| | Fit | 2.20 | 0.14 | 9.53 | - | - | - | 0.97 | 0.38 | 0.82 | 8.86 | 0.96 |
| Interior Shell 02 | Average | 2.36 | 0.17 | 9.59 | 0.20, 31.1 | 0.37, 8.85 | 0.37, 53.0 | 1.23 | 0.35 | 1.62 | 13.41 | 0.34 |
| | Fit | 1.61 | 0.16 | 9.54 | - | - | - | 0.77 | 0.26 | 1.01 | 8.67 | 0.44 |
| O hole | Average | 1.70 | 0.16 | 9.61 | 0.16, 31.1 | 0.28, 5.74 | 0.27, 38.7 | 0.81 | 0.30 | 0.84 | 13.93 | 1.04 |
| | Fit | 1.65 | 0.17 | 9.61 | - | - | - | 0.43 | 0.21 | 0.47 | 5.48 | 0.63 |
| SE Shell 01 | Average | 1.89 | 0.17 | 9.53 | 0.17, 28.3 | 0.40, 8.38 | 0.37, 47.5 | 1.10 | 0.27 | 1.44 | 16.56 | 0.69 |
| | Fit | 2.32 | 0.13 | 9.45 | - | - | - | 0.99 | 0.24 | 1.32 | 12.90 | 0.76 |
| SE Shell 02 | Average | 1.39 | 0.15 | 9.52 | 0.16, 27.5 | 0.51, 10.0 | 0.39, 53.2 | 1.33 | 0.34 | 2.65 | 22.06 | 0.28 |
| | Fit | 1.07 | 0.13 | 9.58 | - | - | - | 1.23 | 0.31 | 1.82 | 17.61 | 0.18 |
| SE Shell 03 | Average | 1.65 | 0.101 | 9.54 | 0.22, 27.4 | 0.64, 9.63 | 0.60, 55.0 | 1.45 | 0.28 | 3.21 | 15.85 | 0.10 |
| | Fit | 1.66 | 0.095 | 9.48 | - | - | - | 1.15 | 0.22 | 2.24 | 11.52 | 0.05 |

NOTE—Average parameters of large regions enclosing some interesting features as denoted in Fig. 7. For each region, the average parameters are calculated in two ways: a direct average based on the parameter images (“Average”) and the parameters obtained by fitting the MOS-1+MOS-2+PN spectra extracted from each region (e.g., Fig. 8) using the model described in Section 3.2.1 (“Fit”). For the former method, kT , $\log n_e t$, and n_e are calculated from Fig. 9(a), (b), and (d). O VII, O VIII, and O VII $K\delta - \zeta$ EWs are calculated from the linear EW maps presented in Fig. 12(a)–(c) (former numbers) and the 2D Spec EW maps presented in Fig. 12(d)–(f) (latter numbers). O, Ne, Mg, Si, and Fe abundances are calculated from the abundance maps in Figs 12(g), 13(c), 14(c), 15(c), and 17(b).

7. ERRATUM: “XMM-Newton large program on SN1006 - II: Thermal emission” (2016, MNRAS, 462, 158)

- $n_{e,\text{ISM}}$ and $n_{e,\text{ejecta}}$ in Table 1 of Li et al. (2016a) should be updated to those in Table 8 of this erratum.

- Fig. 4(e), (f), (h), (i) of Li et al. (2016a) should be updated to the upper left, upper right, lower left, lower right panels of Fig. 4 of this erratum, respectively. Only the scale of the color bars in these figures are changed.

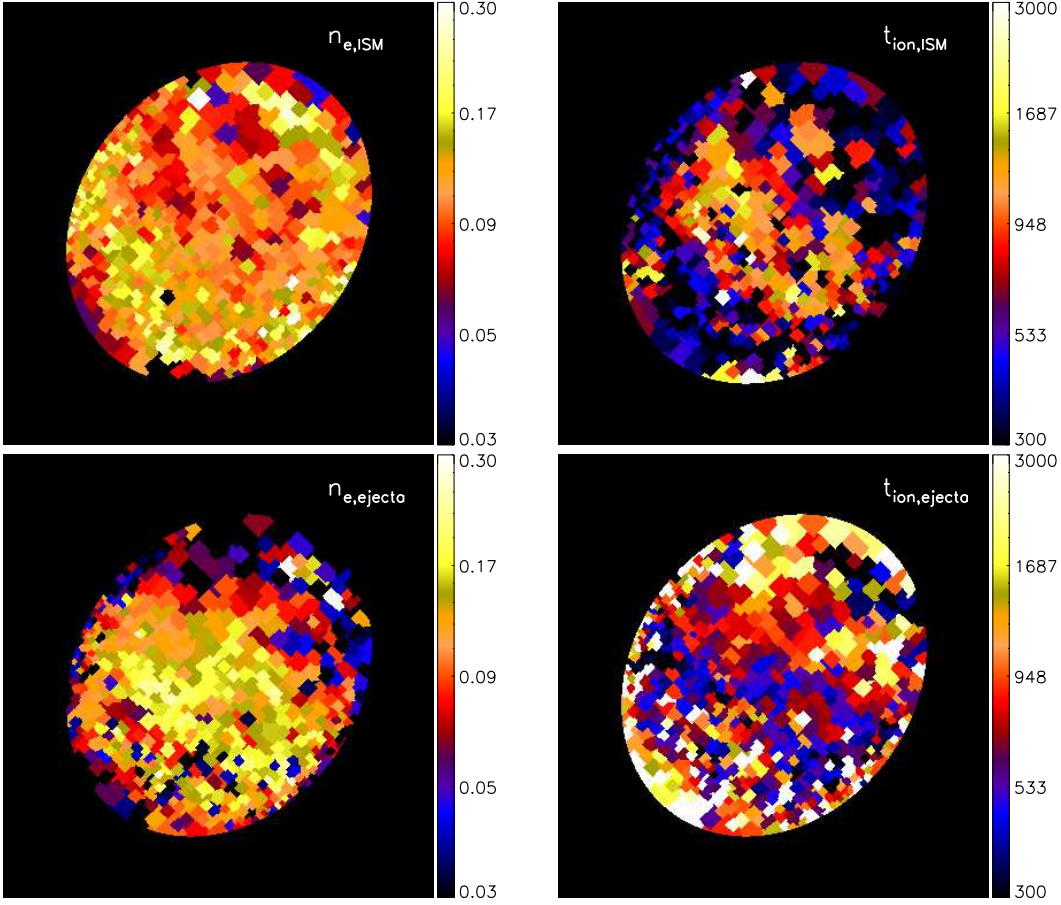


Figure 4. Updated version of Fig. 4(e), (f), (h), (i) of Li et al. (2016a).

8. ERRATUM: “The Circum-Galactic Medium of MASSive Spirals I: Overview and a case study of NGC 5908” (2016, ApJ, 830, 134)

- The following sentences in the abstract of Li et al. (2016b) should be changed to:

“Assuming a metallicity of 0.2 solar, an upper limit (without subtracting the very uncertain young stellar contribution) to the mass of hot gas within this radius is $7.3 \times 10^8 M_{\odot}$. The cooling radius is $r_{\text{cool}} \approx 14 \text{ kpc}$ or $\approx 0.03r_{200}$, within which the hot gas could cool radiatively in less than 10 Gyr, and the cooling of hot gas could significantly contribute in replenishing the gas consumed in star formation. The hot gas accounts for $\approx 5\%$ of the baryons detected within r_{200} .”

- Table 2 of Li et al. (2016b) should be updated to Table 9 of this erratum.

- The last two paragraphs of Section 4.2 of Li et al. (2016b) should be combined together and updated to:

“We further define the cooling radius (r_{cool}) as the radius at which $t_{\text{cool}} = 10 \text{ Gyr}$, within which the hot gas could radiatively cool and be accreted onto the galaxy. From Equation (1), we obtain $t_{\text{cool}} = 10 \text{ Gyr}$ at $n_e \approx 6 \times 10^{-4} \text{ cm}^{-3}$. Since the soft X-ray intensity $I_X \propto n_e^2$, we can estimate the n_e distribution from the hot gas soft X-ray intensity profile (Figure 2), assuming there is no radial variation of the hot gas temperature and metallicity. Adopting the best-fit β -model of the hot gas component, the estimated r_{cool} and the integrated radiative cooling rate within r_{cool} are $r_{\text{cool}} \sim 14 \text{ kpc}$ and $\dot{M}_{\text{hot}} \sim 0.4 (< 1.6) M_{\odot} \text{ yr}^{-1}$. \dot{M}_{hot} , respectively. Considering the large uncertainties in the estimation of both the hot gas properties and the SFR, we may conclude that the radiative cooling of hot gas could at least significantly contribute in replenishing the gas consumed in star formation.”

Table 8. (Table 1 of Li et al. (2016a)) Parameters and errors of the two example regions shown in Fig. 1. Errors are statistical only and are quoted at 90 per cent confidence level.

| Parameter | reg100515 | reg100573 |
|--|---------------------------------------|---------------------------------------|
| $\log(n_e t / \text{cm}^{-3} \text{ s})_{\text{ISM}}$ | $9.320^{+0.034}_{-0.103}$ | $8.948^{+0.220}_{-0.076}$ |
| $n_{e,\text{ISM}} / \text{cm}^{-3}$ | $0.240^{+0.022}_{-0.016}$ | $0.066^{+0.009}_{-0.006}$ |
| $kT_{\text{ejecta}} / \text{keV}$ | $1.29^{+0.25}_{-0.26}$ | > 9.2 |
| $\log(n_e t / \text{cm}^{-3} \text{ s})_{\text{ejecta}}$ | $9.065^{+0.070}_{-0.089}$ | $9.532^{+0.008}_{-0.021}$ |
| $n_{e,\text{ejecta}} / \text{cm}^{-3}$ | $0.082^{+0.016}_{-0.006}$ | $0.085^{+0.006}_{-0.003}$ |
| $Z_{\text{O,ejecta}} / \text{solar}$ | < 20 | $2.39^{+0.74}_{-0.33}$ |
| $(Z_{\text{Ne}} / Z_{\text{O}})_{\text{ejecta}}$ | $0.62^{+0.21}_{-0.19}$ | $0.28^{+0.03}_{-0.02}$ |
| $(Z_{\text{Mg}} / Z_{\text{O}})_{\text{ejecta}}$ | $3.78^{+0.89}_{-0.91}$ | $1.43^{+0.12}_{-0.13}$ |
| $(Z_{\text{Si}} / Z_{\text{O}})_{\text{ejecta}}$ | $13.8^{+9.7}_{-2.8}$ | 3.22 ± 0.33 |
| $(Z_{\text{S}} / Z_{\text{O}})_{\text{ejecta}}$ | $30.1^{+9.1}_{-11.6}$ | $2.21^{+1.51}_{-0.95}$ |
| $(Z_{\text{Fe}} / Z_{\text{O}})_{\text{ejecta}}$ | < 0.39 | < 0.13 |
| $v_{\text{ejecta}} / (\text{km s}^{-1})$ | 1238^{+264}_{-344} | 2818^{+75}_{-443} |
| α | $0.11^{+0.06}_{-0.01}$ | $0.1 (< 0.103)$ |
| $\nu_{\text{cutoff}} / \text{Hz}$ | $7.51^{+0.94}_{-1.22} \times 10^{14}$ | $6.54^{+0.78}_{-0.09} \times 10^{14}$ |
| $\chi^2 / \text{d.o.f.}$ | 704.14/603 | 1417.55/1258 |

Table 9. Inferred parameters of the diffuse hot gas within various radii (Table 2 of Li et al. (2016b))

| | $L_{X,0.5-2\text{keV}}$ $10^{39} \text{ ergs s}^{-1}$ | $\langle n_e \rangle$ $10^{-3} f^{-1/2} \text{ cm}^{-3}$ | M_{hot} $10^9 f^{1/2} M_{\odot}$ | $\langle P_{\text{hot}} \rangle$ $f^{-1/2} \text{ eV cm}^{-3}$ | E_{hot} $10^{57} f^{1/2} \text{ ergs}$ | $\langle t_{\text{cool}} \rangle$ $f^{1/2} \text{ Gyr}$ |
|--|--|---|--|---|--|--|
| $r < 15 \text{ kpc}$ (1.00', 0.036 r_{200}) | $6.83^{+2.73}_{-2.20}$ | $1.95^{+2.41}_{-1.38}$ | $0.73^{+0.90}_{-0.52}$ | $0.73^{+2.44}_{-0.40}$ | $0.43^{+1.43}_{-0.23}$ | 3.1 (< 6.7) |
| $r < 25 \text{ kpc}$ (1.66', 0.06 r_{200}) | $7.09^{+2.83}_{-2.28}$ | $0.93^{+1.15}_{-0.66}$ | $1.59^{+1.96}_{-1.12}$ | $0.35^{+1.17}_{-0.19}$ | $0.93^{+3.11}_{-0.50}$ | 6.5 (< 14.1) |
| $r < 50 \text{ kpc}$ (3.31', 0.12 r_{200}) | $7.28^{+2.91}_{-2.34}$ | $0.33^{+0.41}_{-0.24}$ | $4.55^{+5.63}_{-3.23}$ | $0.13^{+0.42}_{-0.07}$ | $2.67^{+8.90}_{-1.44}$ | 18.0 (< 39.3) |

The hot gas parameters are scaled based on the best-fit X-ray intensity profile of the hot gas component, without subtracting the young stellar contributions. Errors are 1 σ and statistical only. Many systematic uncertainties, such as the poorly constrained metallicity and radial intensity profile at large galactocentric radii, are not included in the errors here. The luminosity L_X , mass (M_{hot}), and thermal energy (E_{hot}) are the total values, while the electron number density (n_e), the thermal pressure (P_{hot}), and the radiative cooling timescale (t_{cool}) are average values.

- As the baryon budget is only meaningful within a large radial range such as r_{200} or the virial radius, we change the title of Section 4.3 of Li et al. (2016b) to “**Baryon Budget**”. The last paragraph of this section should also be changed to:

“Assuming the filling factor $f = 1$, the total baryon mass within the virial radius (described with r_{200}), including the cold atomic and molecular gases, the stars, and the hot gas ($M_{\text{hot}} = 1.44^{+3.27}_{-0.55} \times 10^{10} M_{\odot}$), is $M_b = 2.72^{+0.77}_{-0.70} \times 10^{11} M_{\odot}$. The hot gas only accounts for a small fraction of the total baryon content ($\approx 5\%$). $\sim 80\%$ of the expected baryons are not detected as stars or the cold and hot gas.”

- The following sentences in (2) and (3) of Section 5 of Li et al. (2016b) should be changed to:

“(2) In particular, the cooling radius within which the hot gas could cool radiatively within 10 Gyr is $r_{\text{cool}} \approx 14 \text{ kpc}$, even smaller than the outermost radius where the hot gas emission is directly detected. Within this cooling radius, the total radiative cooling rate of the hot gas is $\dot{M}_{\text{hot}} \sim 0.4 (< 1.6) M_{\odot} \text{ yr}^{-1}$.”

“(3) Adding the mass of cold atomic and molecular gases, hot gas, and stars, the total baryon mass within the virial radius is $M_b \approx 2.72^{+0.77}_{-0.70} \times 10^{11} M_{\odot}$, dominated by the stellar mass. The hot gas only accounts for $\approx 5\%$ of the total baryon content within the virial radius. $\sim 80\%$ of the expected baryons are not detected as stars or the cold and hot gas.”

ACKNOWLEDGMENTS

JTL and RH would like to acknowledge Prof. Joel Bregman from the University of Michigan and Prof. Daniel Wang from the University of Massachusetts for helpful discussions. JTL apologizes to the community on the troubles caused by the mistakes discussed in this paper.

REFERENCES

- Li J.-T., Li Z. Y., Wang Q. D., Irwin J. A., Rossa J., 2008, MNRAS, 390, 59
- Li J.-T., Wang Q. D., Li Z. Y., Chen Y., 2009, ApJ, 706, 693
- Li J.-T., Wang Q. D., 2013, MNRAS, 428, 2085
- Li J.-T., Wang Q. D., Crain R. A., 2014, MNRAS, 440, 859
- Li J.-T., 2015a, MNRAS, 453, 1062
- Li J.-T., Decourchelle A., Miceli M., Vink J., Bocchino F., 2015b, MNRAS, 453, 3953
- Li J.-T., Decourchelle A., Miceli M., Vink J., Bocchino F., 2016a, MNRAS, 462, 158
- Li J.-T., Bregman J. N., Wang Q. D., Crain R. A., Anderson M. E., 2016b, ApJ, 830, 134
- Li J.-T., Bregman J. N., Wang Q. D., Crain R. A., Anderson M. E., Zhang S., 2017, ApJS, 233, 20
- Li J.-T., Bregman J. N., Wang Q. D., Crain R. A., Anderson M. E., 2018, ApJL, 855, 24